A Level-Set Method for Moving Material-Void Interfaces

B. Koren, A.C.J. Venis

A Level-Set Method for Moving Material-Void Interfaces

B. Koren

CWI

P.O. Box 94079, 1090 GB Amsterdam, The Netherlands

A.C.J. Venis

MacNeal-Schwendler (E.D.C.) B.V.

Groningenweg 6, 2803 PV Gouda, The Netherlands

ABSTRACT

This report is a feasibility study of a level-set method for the computation of moving interfaces, in an Eulerian formulation. The report briefly introduces level-set methods and focuses on the development of such a method for moving material-void interfaces. Results are presented for illustrative model problems. As concerns its ability to improve the geometrical resolution of free boundaries, the level-set method appears to perform excellently. Concerning the improvement of other than merely geometrical free-boundary properties, the method performs very well for downstream-facing fronts and is promising for upstream-facing ones.

1. INTRODUCTION

1.1 Problem definition

The subject of this paper is the investigation and further development of a numerical method which is promising for the computation of a special class of free-boundary problems: moving material interfaces, in application areas such as forging, sloshing and explosions in water. Particularly in the first application area, the accuracy requirements imposed on the resolution of the material interface are very high. In some applications, proper use may be made of the property that at one side of the interface, the material can be modeled as void. For example, with steel and air at either side of the interface, the modeling of air as void is quite realistic. In the present paper, the numerical methods considered are not applied to real material-interface problems, but to clarifying model problems with known exact solutions.

1.2 Existing computational approaches

The existing computational approaches for free-boundary problems are Lagrangian, Eulerian or a combination of both: Arbitrary Lagrangian-Eulerian (ALE). In the Lagrangian approach, the grid is attached to the free boundary. As a consequence, the fronts resolved in this way are crisp. But they are not necessarily accurate; their location, even their topology, may be inaccurate. A known drawback of the Lagrangian approach is that it is not well-suited for the computation of bifurcating free boundaries. The Eulerian approach, in which the front moves through a grid which is fixed in space, does not have this drawback, but – as is known – here the fronts are diffused. The ALE technique attempts to avoid both drawbacks. In it, a grid is attached to the front, but it is remeshed in due

time, after great distortions or bifurcations. In case of rapid great distortions or rapid bifurcations, frequent remeshing is needed, which is disadvantageous of course. In the present paper, we consider the pure Eulerian approach only.

In the pure Eulerian approach, since many years, some well-proven techniques exist for computing free-boundary flows. Well-known examples of these are the marker-and-cell (MAC) method (see, for example, [3, 9]) and the volume-of-fluid method (see, for example, [2, 4]). Both methods have as a drawback that they may require intricate (subcell) bookkeeping to properly keep track of fronts. (In case of MAC, the subcell bookkeeping consists of investigating whether possibly occurring cavitating cells are either numerical or physical.) In principle, all this bookkeeping can be avoided in a recently developed class of computing methods for free-boundary flows: the so-called level-set methods [8].

1.3 Level-set methods

Because of their non-smoothness, moving fronts cannot be captured sufficiently accurate on fixed grids. No advantage can be taken of nice numerical accuracy properties, valid for smooth solutions only. As a natural fix to this, in the level-set method, to the system of physical unknowns, a non-physical unknown is added, which *is* smooth at the front: the level-set function. Furthermore, a non-physical equation is added: an advection equation for the level-set function. For example, to the Euler equations written in conservative variables, one may add the level-set function $\psi = \psi(x, y, z, t)$, which is advected as – in principle – a passive scalar, by the likewise conservative equation

$$\frac{\partial(\rho\psi)}{\partial t} + \frac{\partial(\rho u\psi)}{\partial x} + \frac{\partial(\rho v\psi)}{\partial y} + \frac{\partial(\rho w\psi)}{\partial z} = 0. \tag{1.1}$$

This leads to the extended system

$$\frac{\partial q}{\partial t} + \frac{\partial f(q)}{\partial x} + \frac{\partial g(q)}{\partial y} + \frac{\partial h(q)}{\partial z} = 0, \tag{1.2a}$$

$$q = \begin{pmatrix} \rho \\ \rho u \\ \rho v \\ \rho w \\ \rho e \\ \rho\psi \end{pmatrix}, \tag{1.2b}$$

$$f(q) = \begin{pmatrix} \rho u \\ \rho u^2 + p \\ \rho uv \\ \rho uw \\ \rho u(e + \frac{p}{\rho}) \\ \rho u\psi \end{pmatrix}, \quad g(q) = \begin{pmatrix} \rho v \\ \rho vu \\ \rho v^2 + p \\ \rho vw \\ \rho v(e + \frac{p}{\rho}) \\ \rho v\psi \end{pmatrix}, \quad h(q) = \begin{pmatrix} \rho w \\ \rho wu \\ \rho wv \\ \rho w^2 + p \\ \rho w(e + \frac{p}{\rho}) \\ \rho w\psi \end{pmatrix}. \tag{1.2c}$$

Note that in system (1.2), ψ is a passive scalar indeed; there is no feedback of the advection of ψ into that of mass, momentum or energy. In principle, a feedback is not required. In case of a free-boundary computation of, for example, two non-mixing gases at different densities, the standard Eulerian difficulty to accurately resolve the discontinuous gas interface may be alleviated by taking for the level-set function an initial solution which is smooth everywhere (so also at the initial gas interface) and which has a pre-defined and constant value at the interface, a value which exists at the interface only. Then it is clear that to accurately keep track of the gas interface – instead of following the density jump – one can better keep track of this pre-defined interface value for ψ – say ψ_f – because one can take maximal advantage of the smoothness of ψ. (For the density, the accuracy properties of most

higher-order accurate discretizations break down at precisely the point of interest: the interface.) This easy possibility for creating smoothness at the interface (through a smooth, artificial, passive scalar function) is a first interesting property of the level-set method. Related to this, a second interesting property is that the interface location is neatly defined. With a physical jump at the interface, from − say − $c = 1$ to $c = 0$ (where c models, for example, the material density), in case of a diffused grid-representation of this jump, it is not immediately clear how to precisely define the interface location. (Should one define it as there where $c = \frac{1}{2}$ or $c = h$, with h the mesh size, or as whatever?) A third interesting property of the level-set technique is that the level-set function ψ requires no new, specifically tailored discretization method. The discretization method that one has in mind for the physical system, can be easily and consistently extended with the new conservation equation for $\rho\psi$. So, as opposed to fluid markers or volume-of-fluid fractions, the level-set function can be directly and consistently embedded in the existing, discrete system of physical equations. Related to this, a fourth advantage of level-set methods is that there is no difficulty in extending the system of equations from 2-D to 3-D. Finally, a fifth advantage is that in the extended system of discrete equations, one may incorporate a physically sound feedback of the level-set function into the real physical equations. The latter advantage will also be explored in this paper.

The contents of the paper is the following. In Section 2, we present two model problems to be considered throughout this paper and we present reference results for it. In Section 3, the present level-set method is introduced, still without feedback to the physical system. Feedback is introduced − step by step − in Sections 4 and 5. In Section 4, seemingly plausible, but false steps are presented, with results for the two defined test cases. Section 5 describes and evaluates our fed-back level-set method, developed so far for material-void interfaces. Concluding remarks are given in Section 6.

2. Test cases and reference results
2.1 Model problems and exact discrete solutions
In the model problems to be considered, the multi-dimensional advection of an interface is the issue. In here, we are particularly interested in shape preservation of the interface. The problems are described by the 2-D, linear, unsteady advection equation

$$\frac{\partial c}{\partial t} + u\frac{\partial c}{\partial x} + v\frac{\partial c}{\partial y} = 0, \quad (x,y) \in [-1,1] \times [-1,1], \tag{2.1}$$

with as initial conditions:

$$c(x,y,t=0) = \begin{cases} 1, & (x,y) \in (x-x_c)^2 + (y-y_c)^2 \leq d^2, \quad x_c = y_c = -\frac{1}{2}, \quad d = \frac{1}{5}, \\ 0, & \text{elsewhere}, \end{cases} \tag{2.2a}$$

and

$$c(x,y,t=0) = \begin{cases} 1, & (x,y) \in [x_c-d, y_c-d] \times [x_c+d, y_c+d], \quad x_c = y_c = -\frac{1}{2}, \quad d = \frac{1}{5}. \\ 0, & \text{elsewhere}. \end{cases} \tag{2.2b}$$

For the velocity field, defined for positive c only (i.e., in the material only), we simply take

$$u = v = 1, \tag{2.3}$$

and for the inlet boundary conditions we take

$$c(x=-1,y,t) = c(x,y=-1,t) = 0. \tag{2.4}$$

So, the problems describe the diagonal transport in a square domain, of successively a circular initial solution, (2.2a), and a square initial solution, (2.2b). Requested for both the circle and the square: $c(x,y,t=1)$. The exact solutions are identical to the initial solutions, (2.2a) and (2.2b), but now with $x_c = y_c = \frac{1}{2}$. (For other initial values of x_c and y_c, this problem was already considered in [1].)

Both problems are solved on equidistant, cell-centered finite-volume grids with successively 20×20, 40×40 and 80×80 cells, so for $h_x = h_y = h = \frac{1}{10}, \frac{1}{20}$ and $\frac{1}{40}$. Figure 1 shows iso-line distributions of the initial solutions and the final, exact discrete solutions. (The iso-lines are given at $c = 0.1n$, $n = 1, \dots, 9$.)
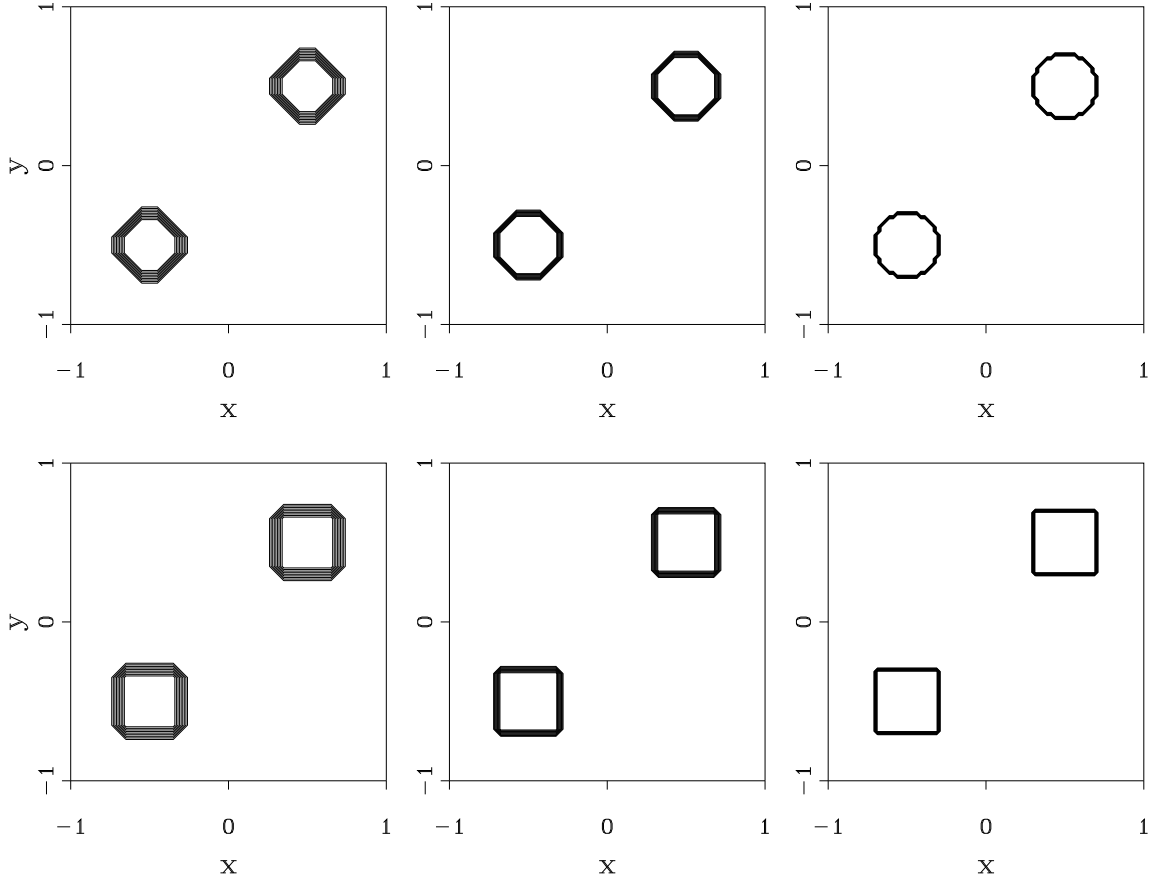
4

Figure 1: Initial and final exact discrete solutions for advection circle (up) and square (down), for from left to right: $h = \frac{1}{10}, \frac{1}{20}, \frac{1}{40}$.

2.2 Standard numerical results
The cell-centered finite-volume discretization of the integral form of (2.1) yields, on an equidistant grid with $h_x = h_y = h$, the semi-discrete equation

$$\frac{1}{h} \iint \frac{\partial c}{\partial t} \mathrm{d}x\mathrm{d}y + u(c_{i+\frac{1}{2},j} - c_{i-\frac{1}{2},j}) + v(c_{i,j+\frac{1}{2}} - c_{i,j-\frac{1}{2}}) = 0. \tag{2.5}$$

In here, the half-integer indices $i-\frac{1}{2},j$ and $i+\frac{1}{2},j$ refer to the vertical cell faces $\partial\Omega_{i-\frac{1}{2},j}$ and $\partial\Omega_{i+\frac{1}{2},j}$, in between the cells $\Omega_{i-1,j}$ and $\Omega_{i,j}$, and $\Omega_{i,j}$ and $\Omega_{i+1,j}$, respectively (Figure 2). Likewise, the indices $i, j - \frac{1}{2}$ and $i, j + \frac{1}{2}$ refer to the horizontal cell faces $\partial\Omega_{i,j-\frac{1}{2}}$ and $\partial\Omega_{i,j+\frac{1}{2}}$, separating $\Omega_{i,j-1}$ and $\Omega_{i,j}$, and $\Omega_{i,j}$ and $\Omega_{i,j+1}$ (Figure 2).

We proceed by giving the standard numerical scheme for computing the cell-face fluxes in the present two problems. At the vertical cell faces we apply

$$c_{i+\frac{1}{2},j} = \begin{cases} i = 0: & (c_{\text{exact}})_{\frac{1}{2},j} = 0, \\ i = 1: & \frac{1}{2}(c_{1,j} + c_{2,j}), \\ i = n: & c_{n,j} + \frac{1}{2}(c_{n,j} - c_{n-1,j}), \\ \text{else}: & c_{i,j} + \frac{1}{2}\phi(r_{i+\frac{1}{2},j})(c_{i,j} - c_{i-1,j}), \quad r_{i+\frac{1}{2},j} \equiv \frac{c_{i+1,j}-c_{i,j}+\epsilon}{c_{i,j}-c_{i-1,j}+\epsilon}, \quad 0 < \epsilon \ll 1, \end{cases} \tag{2.6a}$$
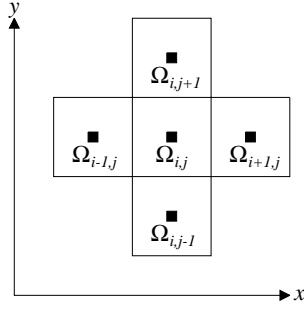
Figure 2: Cell-centered finite volume $\Omega_{i,j}$ with nearest neighbors.

and likewise, at the horizontal cell faces

$$
c_{i,j+\frac{1}{2}} = \begin{cases}
j = 0 : & (c_{\mathrm{exact}})_{i,\frac{1}{2}} = 0. \\
j = 1 : & \frac{1}{2}(c_{i,1} + c_{i,2}). \\
j = n : & c_{i,n} + \frac{1}{2}(c_{i,n} - c_{i,n-1}). \\
\text{else} : & c_{i,j} + \frac{1}{2}\phi(r_{i,j+\frac{1}{2}})(c_{i,j} - c_{i,j-1}), \quad r_{i,j+\frac{1}{2}} \equiv \frac{c_{i,j+1} - c_{i,j} + \epsilon}{c_{i,j} - c_{i,j-1} + \epsilon}, \quad 0 < \epsilon \ll 1.
\end{cases}
\tag{2.6b}
$$

As the limiter $\phi = \phi(r)$, we apply

$$
\phi(r) = \begin{cases}
0, & r < 0. \\
2r, & r < \frac{2}{5}. \\
\frac{4}{5}, & r < \frac{7}{10}. \\
\frac{1}{3} + \frac{2}{3}r, & r < \frac{5}{2}. \\
2, & \text{else.}
\end{cases}
\tag{2.7}
$$

This limiter is an improved version of the $\kappa = \frac{1}{3}$-limiter presented in [5]. While the $\kappa = \frac{1}{3}$-limiter from [5] is formally third-order accurate in monotonous, smooth flow parts only, the new $\kappa = \frac{1}{3}$-limiter (2.7) also gives third-order accuracy in smooth extrema. The standard space discretization has been defined now.

For the time integration we simply take the standard, four-stage Runge-Kutta scheme, which is fourth-order time-accurate for nonlinear problems. In all computational results to be presented hereafter, the time step is taken linearly proportional to the mesh size, and sufficiently small to ensure that time discretization errors are negligible with respect to space discretization errors. (Stability and monotonicity are guaranteed by these small time steps.)

In Figure 3, as in Figure 1, we give the iso-line distributions of the initial and final solutions. (Iso-lines are given again at $c = 0.1n$, $n = 1, \dots, 9$.) In Table 1 (p. 22), some more quantitative information is given about these numerical solutions. In here, $\|\Delta c\|_1$ and $\|\Delta c\|_\infty$ are the L_1- and L_∞-norms of the solution errors. Due to the non-smoothness of both initial solutions we do not observe a higher than $\mathcal{O}(h)$ accuracy behavior in $\|\Delta c\|_1$. (The error $\|\Delta c\|_\infty$ behaves even zeroth-order accurate only.)

3. PRESENT LEVEL-SET METHOD
3.1 Principle
To explain the principle of the present level-set method, for transparency reasons we consider the 1-D advection equation

$$
\frac{\partial c}{\partial t} + u \frac{\partial c}{\partial x} = 0, \quad u = \text{constant} > 0.
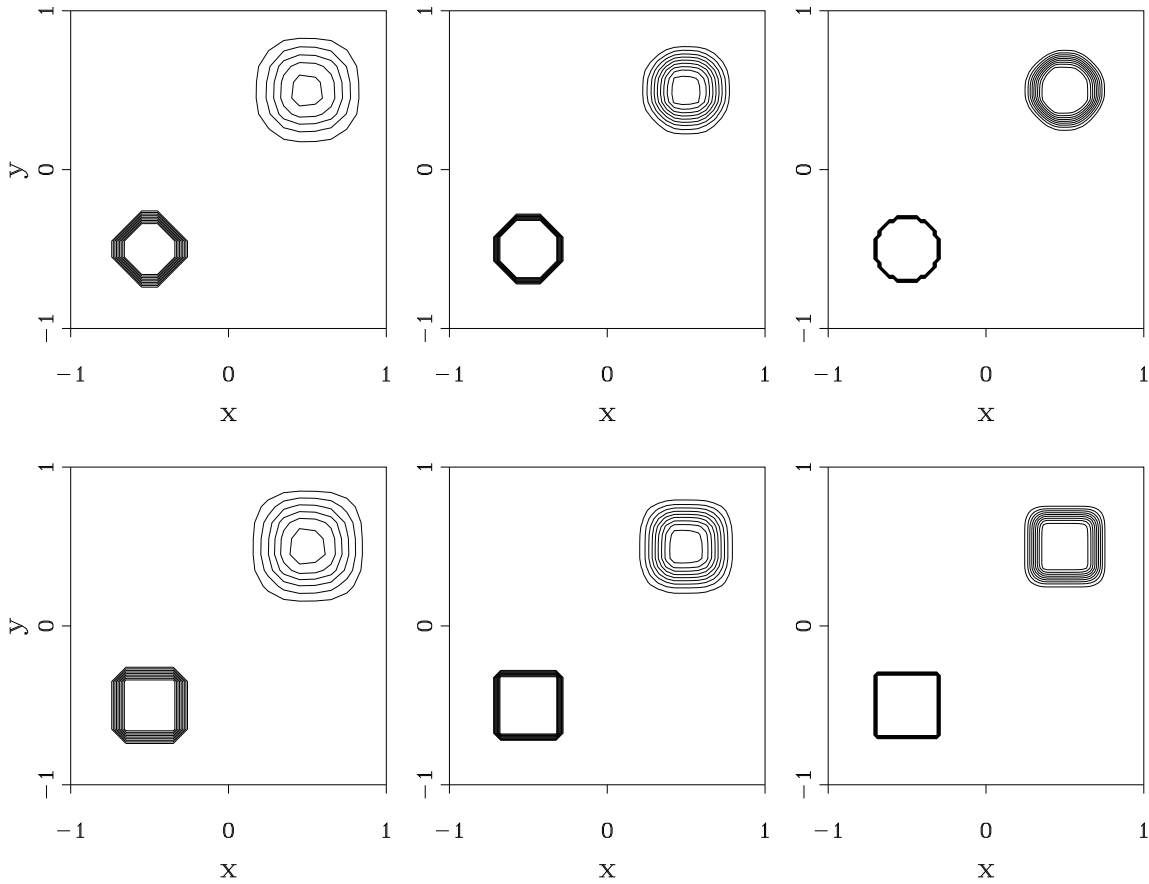\tag{3.1}
$$

Figure 3: Initial and final numerical solutions for advection circle (up) and square (down) with limited $\kappa = \frac{1}{3}$-scheme, for from left to right: $h = \frac{1}{10}, \frac{1}{20}, \frac{1}{40}$.

Denoting the level-set function again by ψ, the extended equation reads

$$\frac{\partial q}{\partial t} + u\frac{\partial q}{\partial x} = 0, \quad q = \begin{pmatrix} c \\ \psi \end{pmatrix}, \quad u = \text{constant} > 0. \tag{3.2}$$

Suppose that the initial solution $c(x, t = 0)$ looks as in the sketch in Figure 4a, so with the interface at $x = x_f$ and a jump from $c = 1$ to $c = 0$ over there. Then, for the corresponding initial distribution of the level-set function, $\psi(x, t = 0)$, we propose the probability curve

$$\psi(x, t = 0) = e^{-\frac{1}{2}\left(\frac{x}{x_f}\right)^2}. \tag{3.3}$$

A sketch of (3.3) is given in Figure 4b. Note that level-set function (3.3) is infinitely many times differentiable; higher-order accurate advection schemes can take full advantage of this. Further note that the function has been chosen such that its inflection point (its maximum slope) coincides with the interface. (This gives the best posedness of the interface-detection problem.) In the level-set method, for the present 1-D model equation, a front is embedded in a 1-D function, while the front itself is a 0-D (a point) phenomenon only. This is typical for level-set methods: n-D physical fronts ($n = 0, 1$ or 2) are embedded in $(n + 1)$-D functions. (This is the price to be paid for the advantages mentioned in Section 1.3.) We still remark that the choice (3.3) for the level-set function is rather arbitrary.

Other functions, with equally good differentiation properties, and interface values ψ_f different from $\frac{1}{\sqrt{e}}$, could have been chosen. For example, $\psi_f = 0$ with the level-set function running from $1 - \frac{1}{\sqrt{e}}$ to $-\frac{1}{\sqrt{e}}$, instead of from 1 to 0, may lead to a slightly improved computational efficiency. (However, for the real physical applications we have in mind, underwater explosions for example, this will be a micro-gain in efficiency only.)

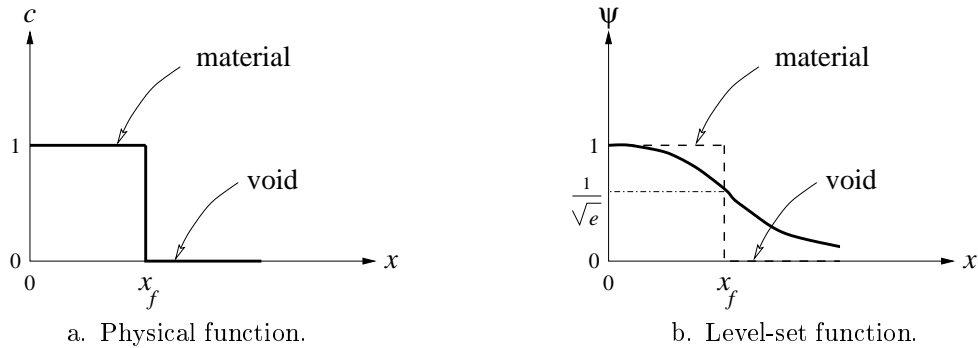a. Physical function. b. Level-set function.

Figure 4: Initial solutions.

For a multi-D problem, for instance, the 2-D problem of which the initial material-void interface is sketched in Figure 5, the choice of the initial level-set function may be done in the following way. Take some point in the material and define that as the origin of a local r, ϕ-coordinate system (Figure 5). Next take as the initial level-set function

$$\psi(r, \phi, t = 0) = e^{-\frac{1}{2}\left(\frac{r}{r_f}\right)^2}, \tag{3.4}$$

where $r_f = r_f(\phi)$ is the radial distance from the point chosen to the material interface, for a given angle ϕ, $\phi \in [0, 2\pi]$. Doing so, we have $\psi_f = \frac{1}{\sqrt{e}}$ all over the interface. For many shapes, this initialization works, also in 3-D, where it carries over in a spherical coordinate system.
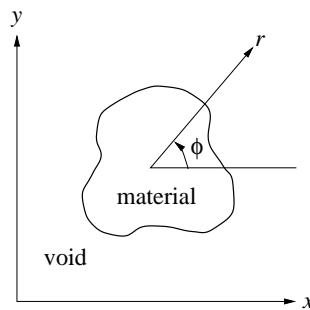

Figure 5: 2-D material-void interface.

3.2 Velocity field

A subtle property of the advection of material-void interfaces is that the velocity field is only defined in the material. Hence, for the advection of the level-set function in the void region, an artificial velocity field still has to be defined. The opportunity to make this choice, without being inhibited by physics, is a good chance in fact to improve the free boundary's resolution. For example, in the void region an artificial velocity can be chosen which counteracts the effects of numerical diffusion of the physical quantity c. For the 1-D advection equation (3.1), in the void region a velocity may be

defined which looks as sketched in Figures 6a and 6b. So, for a downstream-facing front, $u\frac{\partial \psi}{\partial x} < 0$, at the void side of the interface, a velocity may be chosen which is smaller than the velocity at the material side of the interface. This artificial anti-advection implies converging characteristics and may thus lead to re-steepening of a diffused front. To realize the steepening in case of an upstream-facing front, $u\frac{\partial \psi}{\partial x} > 0$, the void velocity has to be taken greater than the material velocity (Figure 6b).

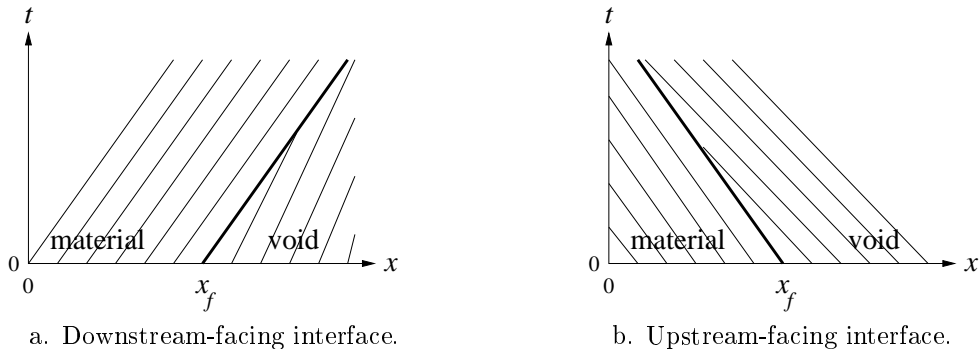a. Downstream-facing interface.   b. Upstream-facing interface.

Figure 6: Anti-advection for moving material-void interfaces.

Of course, a difficulty here is to not affect too seriously the physically correct propagation speed of the front. Another difficulty of the approach is to maintain the smoothness of the level-set function at the interface. Therefore, in this paper we do not apply anti-advection. (In [1], the idea of anti-advection *has* been applied.) Our present suggestion for the choice of the artificial velocity field in the void region is to take that as the smoothest possible extrapolation of the velocity field at the material interface. In case of a constant velocity at the interface, one defines that specific velocity as the velocity in the entire void region. In case of a non-constant velocity at the interface, we suggest to take that velocity distribution, say $q_{\mathrm{in}} = q_{\mathrm{in}}(\phi)$ (Figure 7) as the inner boundary condition for an elliptic boundary-value problem, defined for the artificial velocity in the void region. As the boundary condition at the outer boundary of the void region, q_{out} (Figure 7), we take the average velocity at the material interface. So, in 2-D, this elliptic velocity generator amounts to solving

$$\Delta q = 0, \quad q = \begin{pmatrix} u \\ v \end{pmatrix}, \quad q_{\mathrm{in}} = q_{\mathrm{in}}(\phi), \quad q_{\mathrm{out}} = \frac{1}{2\pi} \int_0^{2\pi} q_{\mathrm{in}}(\phi)\mathrm{d}\phi. \tag{3.5}$$
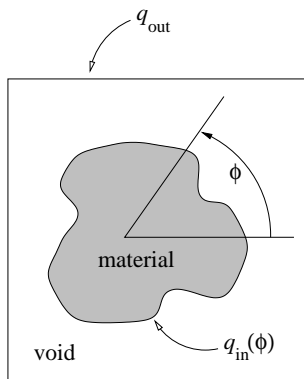

Figure 7: Void region.

4. Simple level-set results: shape tracking only
For the two test cases defined in Section 2.1, we can already present practically relevant level-set results now, viz. for the advection of the shape. As the local origins of the r, ϕ-coordinate system introduced in Section 3.1, we simply take the centers of gravity of the initial circle and the initial square. For the initial function $\psi(r, \phi, t = 0)$ we take (3.4) and for its numerical advection scheme the non-limited $\kappa = \frac{1}{3}$-scheme. So – as mentioned – the level-set function is simply embedded into the existing discretization, with as the only difference that for the level-set function the limiter is switched off. Thus, for clearness, at the vertical cell faces we take

$$
\psi_{i+\frac{1}{2},j} = \begin{cases}
i = 0: & (\psi_{\text{exact}})_{\frac{1}{2},j} = e^{-\frac{1}{2}\left(\frac{r_{\frac{1}{2},j}(t)}{r_f(t)}\right)^2}, \\
i = 1: & \frac{1}{2}(\psi_{1,j} + \psi_{2,j}), \\
i = n: & \psi_{n,j} + \frac{1}{2}(\psi_{n,j} - \psi_{n-1,j}), \\
\text{else}: & \psi_{i,j} + \frac{1+\kappa}{4}(\psi_{i+1,j} - \psi_{i,j}) + \frac{1-\kappa}{4}(\psi_{i,j} - \psi_{i-1,j}), \quad \kappa = \frac{1}{3},
\end{cases}
\tag{4.1a}
$$

and likewise, at the horizontal cell faces

$$
\psi_{i,j+\frac{1}{2}} = \begin{cases}
j = 0: & (\psi_{\text{exact}})_{i,\frac{1}{2}} = e^{-\frac{1}{2}\left(\frac{r_{i,\frac{1}{2}}(t)}{r_f(t)}\right)^2}, \\
j = 1: & \frac{1}{2}(\psi_{i,1} + \psi_{i,2}), \\
j = n: & \psi_{i,n} + \frac{1}{2}(\psi_{i,n} - \psi_{i,n-1}), \\
\text{else}: & \psi_{i,j} + \frac{1+\kappa}{4}(\psi_{i,j+1} - \psi_{i,j}) + \frac{1-\kappa}{4}(\psi_{i,j} - \psi_{i,j-1}), \quad \kappa = \frac{1}{3},
\end{cases}
\tag{4.1b}
$$

with the radii $r_{\frac{1}{2},j}(t)$, $r_{i,\frac{1}{2}}(t)$ and $r_f(t)$ exact for both the circular and the square shape. Applying the identical time integration as in Section 2.2, we obtain the results depicted in Figure 8.

As in Table 1, in Table 2 (p. 22), we give some more quantitative information about the numerical level-set solutions. As expected, we *do* have higher-order accuracy here. For the circular shape, both $\|\Delta\psi\|_1$ and $\|\Delta\psi\|_\infty$ behave almost third-order accurate. For the square solution, due to the non-smoothness at the four corners, the accuracy behavior is less good: second-order almost, which is still better nevertheless than the order of accuracy to be observed in Table 1.

We also have the possibility now to compare the shape preservation properties of both approaches: the standard numerical approach from Section 2.2 and the present level-set approach. For additional comparison purposes, we also consider the corresponding, exact discrete solutions. For both the exact discrete solution and the solution obtained by the standard approach, we define the material interface as the location where $c_f \equiv h$ (h being the mesh width). Note that in the standard approach – as mentioned in Section 1.3 – just a proper definition of the material interface is not trivial already. In the level-set approach, this definition already exists: $\psi_f \equiv \frac{1}{\sqrt{e}}$. For the 80×80-grid, in Figure 9, we present discrete shapes at $t = 1$, from left to right: (i) according to the exact discrete solution c (the iso-line $c = c_f = h$), (ii) according to the limited $\kappa = \frac{1}{3}$ solution c (the iso-line $c = c_f = h$ as well) and (iii) according to the non-limited $\kappa = \frac{1}{3}$ solution ψ (the iso-line $\psi = \psi_f = \frac{1}{\sqrt{e}}$). (The iso-lines in the two most left graphs of Figure 9 belong to the same solutions that have already been depicted in the two most right graphs of Figure 1, and – likewise – the two middle graphs in Figure 9 belong to the same solutions already depicted in the two most right graphs in Figure 3.) For the circle, the difference in quality between the standard numerical results and the level-set results is striking. Seen from Figure 9, the shape preservation of the level-set circle is very good; numerical errors are very small. The depicted level-set circle is even more accurate than the plotted, exact discrete circle! The quality of the latter suffers from the interface-definition problem. For the square, the level-set solution is less accurate than for the circle (because of the loss of one order of accuracy caused by the corners). Nevertheless, here as well, the level-set result is still much better than the standard numerical result in the middle graph. Thus, one of the major goals of this work, good shape preservation of interfaces, has already been obtained now.
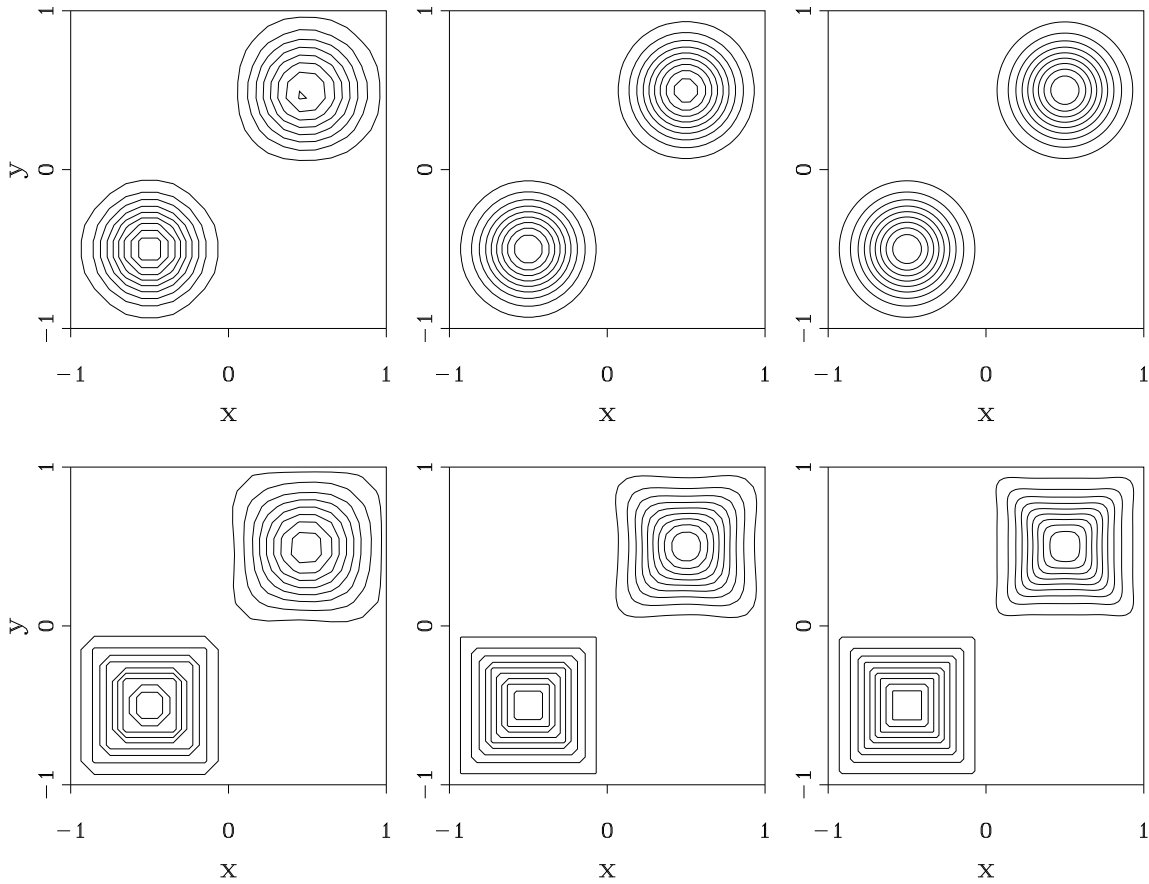
Figure 8: Initial and final numerical solutions for advection circular (up) and square (down) level-set function ψ with non-limited $\kappa = \frac{1}{3}$-scheme, for from left to right: $h = \frac{1}{10}, \frac{1}{20}, \frac{1}{40}$.

5. Extended level-set results: feedback with physics

The level-set results presented in the previous section are very worthwhile. However, in practical applications, shape preservation may not be the only goal. An accurate resolution of physical quantities at the interface may also be of interest. For example, in a real fluid dynamics problem, the velocity components at the interface are a particularly important issue, since they determine the motion of the free surface. Also, the density distribution along and near the interface may be of interest. Note that, so far, we do have obtained good shape preservation (the two right graphs in Figure 9), but a physical quantity as density will still be diffused at the interface (as demonstrated in the two middle graphs of Figure 9). However, with the level-set function and equation added to a system of physical conservation laws, the useful knowledge to be extracted from the numerical solution of the level-set function does not need to be restricted to geometrical improvement of the free boundary only. Knowledge obtained from the level-set solution can also be fed back into the discretization of the physical equations. This feedback of the level-set function to physics is application-dependent and much effort may be put into it. Already for the present model for moving material-void interfaces, despite the model's simplicity, it will appear that defining the feedback is not straightforward; many possibilities exist. We proceed by presenting feedback schemes with increasing complexity, but − also − with increasing solution quality. The first schemes are wrong, but are presented for illustrative
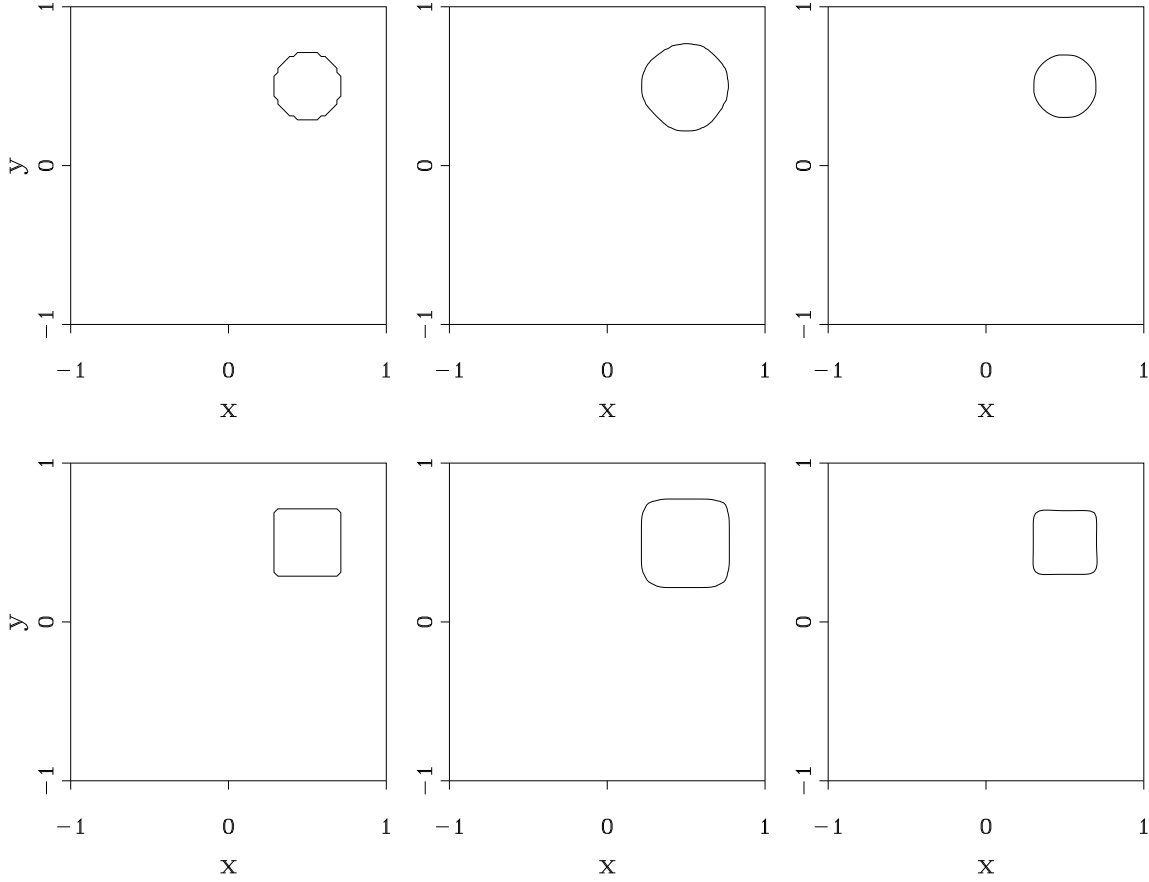
Figure 9: Final shapes for circle (up) and square (down), for $h = \frac{1}{40}$ and according to, from left to right: exact discrete solution c (iso-line $c = c_f = h$), limited $\kappa = \frac{1}{3}$-solution c (iso-line $c = c_f = h$) and non-limited $\kappa = \frac{1}{3}$-solution ψ (iso-line $\psi = \psi_f = \frac{1}{\sqrt{e}}$).

purposes. The model equation to be considered in the following is

$$\frac{\partial q}{\partial t} + u\frac{\partial q}{\partial x} + v\frac{\partial q}{\partial y} = 0, \quad q = \begin{pmatrix} c \\ \psi \end{pmatrix}, \quad u = v = 1. \tag{5.1}$$

5.1 Wrong discrete schemes for feedback of level-set function to advection material interface

First wrong feedback The decoupled discretization of system (5.1) is given by (2.6), (2.7) and (4.1). In making the physical coupling, we maintain discretization (4.1) for the level-set function, but we extend (2.6). A (seemingly) obvious physical argument for making this extension for the present (model) interfaces is that in the void region, the physical fluxes must be zero. The direct implementation of this into the discretization of c leads, for the vertical and horizontal cell faces, respectively, to

$$c_{i+\frac{1}{2},j} = \max\left(0, \frac{\psi_{i+\frac{1}{2},j} - \psi_f}{|\psi_{i+\frac{1}{2},j} - \psi_f|}\right) c_{i+\frac{1}{2},j}, \tag{5.2a}$$

$$c_{i,j+\frac{1}{2}} = \max\left(0, \frac{\psi_{i,j+\frac{1}{2}} - \psi_f}{|\psi_{i,j+\frac{1}{2}} - \psi_f|}\right) c_{i,j+\frac{1}{2}}, \tag{5.2b}$$

where $c_{i+\frac{1}{2},j}$ and $c_{i,j+\frac{1}{2}}$ in the righthand sides are determined by (2.6) with limiter (2.7), and $\psi_{i+\frac{1}{2},j}$ and $\psi_{i,j+\frac{1}{2}}$ by (4.1). So, note that in (5.2), in fact, an extra limiting is applied to the physical fluxes, a limiting controlled by the level-set function. The level-set limiting is binary; it either opens or closes cell faces. In the void region ($\psi < \psi_f$) it closes all cell faces. This obviously inhibits numerical diffusion into the void region. Note that to still preserve monotonicity, the original limiter $\phi(r)$ is still necessary, of course. Since the binary limiter can have the values zero and one only, it cannot affect this monotonicity. For clearness we also remark that the level-set limiter, with its ability to close cell faces, does not affect conservation; the basic finite-volume scheme remains unchanged. (What flows out of or into a cell across a face, remains to flow into or out of the cell neighboring that face.)

Numerical results obtained with this first feedback scheme for the two test cases, are given in Figure 10. To show the failure of the scheme, here we refrained from depicting the initial solution. Small amounts of mass stagnate; they are pent up in cells with faces closed by the level-set limiter. The cause is clear; if in a cell $\Omega_{i,j}$, $\psi_{i-\frac{1}{2},j}$, $\psi_{i+\frac{1}{2},j}$, $\psi_{i,j-\frac{1}{2}}$ as well as $\psi_{i,j+\frac{1}{2}}$ are less than ψ_f, all four corresponding cell faces ($\partial\Omega_{i-\frac{1}{2},j}$, $\partial\Omega_{i+\frac{1}{2},j}$, $\partial\Omega_{i,j-\frac{1}{2}}$ and $\partial\Omega_{i,j+\frac{1}{2}}$) are closed, irrespective of the fact that there is still some mass in that cell ($c_{i,j} > 0$). For clarity, in Figure 11 we depicted this undesired situation. A straightforward fix is to apply a flux correction to cells where this situation occurs. In the next section we work out this remedy and present numerical results for it.

First wrong feedback extended with flux correction   After having computed all cell-face fluxes, but not yet the net cell fluxes, in each cell $\Omega_{i,j}$ we may check if

$$c_{i-\frac{1}{2},j} = c_{i+\frac{1}{2},j} = c_{i,j-\frac{1}{2}} = c_{i,j+\frac{1}{2}} = 0, \quad \text{while } c_{i,j} > h^2. \tag{5.3}$$

If situation (5.3) occurs in a cell, that cell has been improperly closed; the mass in it has been erroneously locked up, and will remain to be so in our test cases, if we do not change the scheme developed so far. The remedy for such a particular cell is to recompute all four cell face values $c_{i-\frac{1}{2},j}$, $c_{i+\frac{1}{2},j}$, $c_{i,j-\frac{1}{2}}$ and $c_{i,j+\frac{1}{2}}$ by the standard scheme (2.6)–(2.7). After having done so for all cells where this is needed, the cell-face fluxes can be finally assembled to the net cell fluxes. (Note that by starting to correct the cell-face fluxes and not directly the net cell fluxes, the scheme remains conservative.)

Doing so, we obtain the results given in Figure 12. The stagnation problem has been solved (all mass flows now), but the solution accuracy is still unacceptable. It seems that certain cell faces near the upstream-facing part of both shapes are closed for mass that has been diffused into the wake. In the next section, we propose a possible fix to this.

Second wrong feedback   A weak spot of the level-set-based feedback developed so far is still hidden in the case of a multi-D situation as sketched in Figure 13, i.e., a situation in which the iso-line $\psi = \psi_f$ (the material interface) cuts the cell face considered and where the corresponding cell-face value – say $\psi_{i+\frac{1}{2},j}$ – is less than ψ_f.

In such a case, the level-set limiter applied so far, closes that cell face by setting $c_{i+\frac{1}{2},j}$ to zero, which is wrong of course. In this case the cell face should be left open. I.e., the level-set limiter value should be 1 instead of 0. To realize this, we propose the following improved level-set limiter. First, we approximate the cell-vertex values ψ_1 and ψ_2 (Figure 13). For the vertical cell face $\partial\Omega_{i+\frac{1}{2},j}$, these node values can be approximated by

$$(\psi_1)_{i+\frac{1}{2},j} = \begin{cases} j = 1: & \psi_{i+\frac{1}{2},1} + \frac{1}{2}(\psi_{i+\frac{1}{2},1} - \psi_{i+\frac{1}{2},2}), \\ \text{else}: & \frac{1}{2}(\psi_{i+\frac{1}{2},j-1} + \psi_{i+\frac{1}{2},j}), \end{cases} \tag{5.4a}$$

$$(\psi_2)_{i+\frac{1}{2},j} = \begin{cases} j = n: & \psi_{i+\frac{1}{2},n} + \frac{1}{2}(\psi_{i+\frac{1}{2},n} - \psi_{i+\frac{1}{2},n-1}), \\ \text{else}: & \frac{1}{2}(\psi_{i+\frac{1}{2},j} + \psi_{i+\frac{1}{2},j+1}), \end{cases} \tag{5.4b}$$
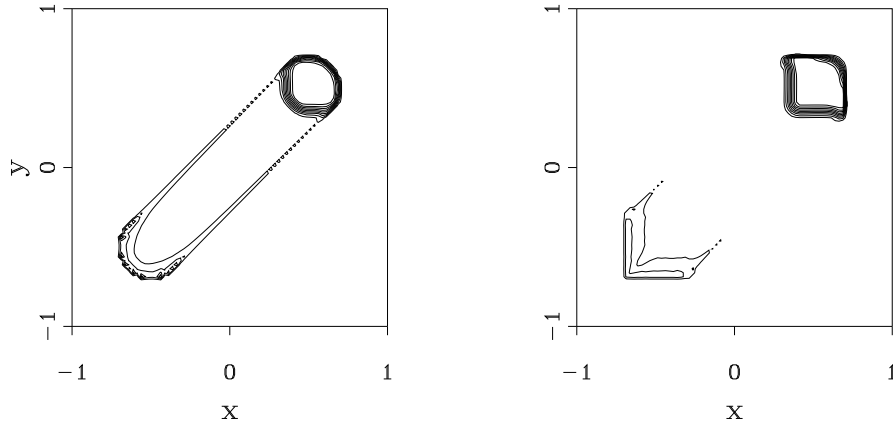
Figure 10: Initial and final numerical solutions (c) for advection circle (left) and square (right) with first wrong feedback of level-set function to physics ($h = \frac{1}{40}$).
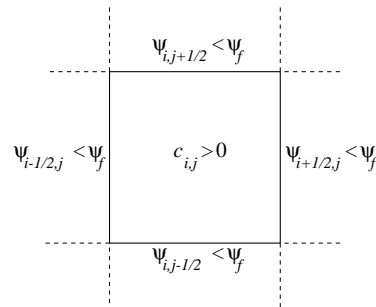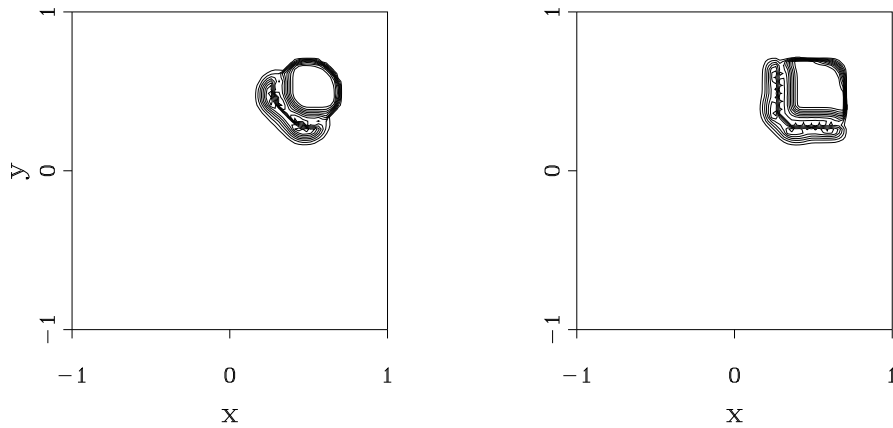

Figure 11: Pent up mass.

Figure 12: Initial and final numerical solutions (c) for advection circle (left) and square (right) with first wrong feedback of level-set function to physics and with flux correction ($h = \frac{1}{40}$).
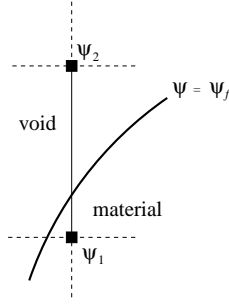
14

Figure 13: Material-void interface cutting cell face.

with $\psi_{i+\frac{1}{2},j}$ according to (4.1a). For the horizontal cell face $\partial\Omega_{i,j+\frac{1}{2}}$ we have

$$(\psi_1)_{i,j+\frac{1}{2}} = \begin{cases} i = 1: & \psi_{1,j+\frac{1}{2}} + \frac{1}{2}(\psi_{1,j+\frac{1}{2}} - \psi_{2,j+\frac{1}{2}}), \\ \text{else}: & \frac{1}{2}(\psi_{i-1,j+\frac{1}{2}} + \psi_{i,j+\frac{1}{2}}), \end{cases} \quad (5.5a)$$

$$(\psi_2)_{i,j+\frac{1}{2}} = \begin{cases} i = n: & \psi_{n,j+\frac{1}{2}} + \frac{1}{2}(\psi_{n,j+\frac{1}{2}} - \psi_{n-1,j+\frac{1}{2}}), \\ \text{else}: & \frac{1}{2}(\psi_{i,j+\frac{1}{2}} + \psi_{i+1,j+\frac{1}{2}}), \end{cases} \quad (5.5b)$$

with $\psi_{i,j+\frac{1}{2}}$ according to (4.1b). Then, at the vertical cell face $\partial\Omega_{i+\frac{1}{2},j}$, the improved scheme is

$$c_{i+\frac{1}{2},j} = \begin{cases} \left((\psi_1)_{i+\frac{1}{2},j} - \psi_f\right)\left((\psi_2)_{i+\frac{1}{2},j} - \psi_f\right) < 0: & \text{according to (2.6a) and (2.7),} \\ \text{else}: & \text{according to (5.2a),} \end{cases} \quad (5.6a)$$

and at the horizontal cell face $\partial\Omega_{i,j+\frac{1}{2}}$

$$c_{i,j+\frac{1}{2}} = \begin{cases} \left((\psi_1)_{i,j+\frac{1}{2}} - \psi_f\right)\left((\psi_2)_{i,j+\frac{1}{2}} - \psi_f\right) < 0: & \text{according to (2.6b) and (2.7).} \\ \text{else}: & \text{according to (5.2b).} \end{cases} \quad (5.6b)$$

This improved level-set limiting can be applied with and without the flux correction proposed in Section 5.1. In Figures 14 and 15, we present results for the two test cases. As it appears from the figures, the improvement has not paid off. In all four figures, still, an erroneous spray of mass is observed in the wake.

5.2 Improved feedback of level-set function to advection material-void interface
Distinction between downstream- and upstream-facing fronts   Inspecting all previous results obtained with the level-set feedback (Figures 10, 12, 14 and 15), it appears there is a clear difference in solution quality at the downstream- and the upstream-facing interfaces. The closure of cell faces in the void region appears to make sense for the resolution of downstream-facing fronts, but not for the upstream-facing ones. We can clearly illustrate this by means of the following simplifications of the two model problems. The equation and velocity to be considered are still the same, i.e., (2.1) and (2.3), respectively, but the initial solutions differ. Instead of (2.2a), first we consider a downstream-facing curvilinear front only, viz.

$$c(x,y,t=0) = \begin{cases} 1, & (x,y) \in (x - x_c)^2 + (y - y_c)^2 \leq d^2, \quad x_c = y_c = -1, \quad d = \frac{1}{2}, \\ 0, & \text{elsewhere,} \end{cases} \quad (5.7a)$$

and likewise, instead of (2.2b), the downstream-facing rectilinear front

$$c(x,y,t=0) = \begin{cases} 1, & (x,y) \in [x_c, y_c] \times [x_c + d, y_c + d], \quad x_c = y_c = -1, \quad d = \frac{1}{2}. \\ 0, & \text{elsewhere.} \end{cases} \quad (5.7b)$$
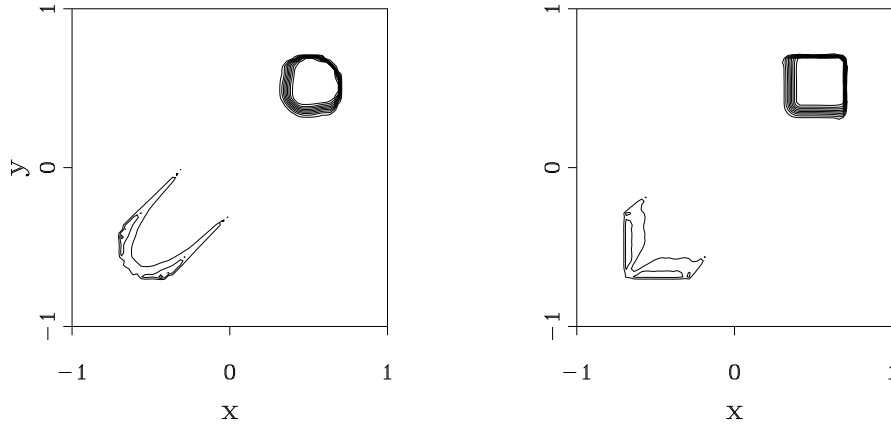
Figure 14: Final numerical solutions (c) for advection circle (left) and square (right) with second wrong feedback of level-set function to physics ($h = \frac{1}{40}$).
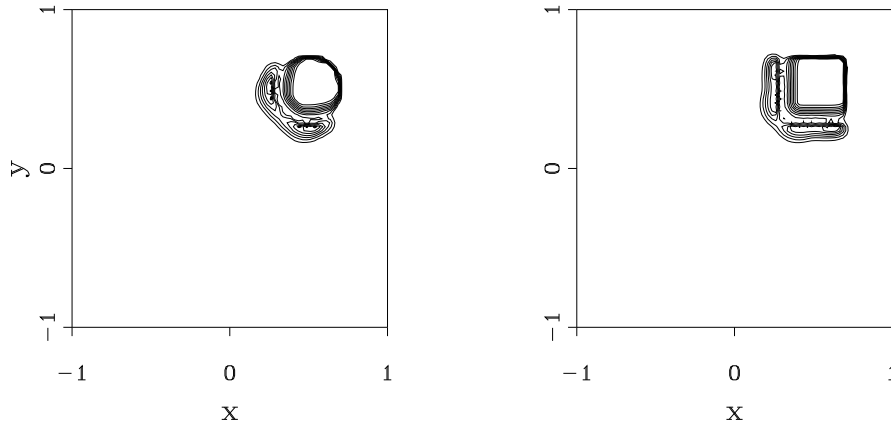

Figure 15: Final numerical solutions (c) for advection circle (left) and square (right) with second wrong feedback of level-set function to physics and with flux correction ($h = \frac{1}{40}$).

For both fronts, the corresponding boundary conditions are

$$c(x = -1, y, t) = \begin{cases} 1, & y \le (y_c + d) + vt, \\ 0, & \text{elsewhere,} \end{cases} \tag{5.8a}$$

$$c(x, y = -1, t) = \begin{cases} 1, & x \le (x_c + d) + ut. \\ 0, & \text{elsewhere.} \end{cases} \tag{5.8b}$$

Vice versa, we consider the upstream-facing analogies:

$$c(x, y, t = 0) = \begin{cases} 0, & (x, y) \in (x - x_c)^2 + (y - y_c)^2 \le d^2, \quad x_c = y_c = -1, \quad d = \frac{1}{2}, \\ 1, & \text{elsewhere,} \end{cases} \tag{5.9a}$$

and

$$c(x, y, t = 0) = \begin{cases} 0, & (x, y) \in [x_c, y_c] \times [x_c + d, y_c + d], \quad x_c = y_c = -1, \quad d = \frac{1}{2}, \\ 1, & \text{elsewhere,} \end{cases} \tag{5.9b}$$

both with

$$c(x = -1, y, t) = \begin{cases} 0, & y \leq (y_c + d) + vt, \\ 1, & \text{elsewhere,} \end{cases} \tag{5.10a}$$

$$c(x, y = -1, t) = \begin{cases} 0, & x \leq (x_c + d) + ut. \\ 1, & \text{elsewhere.} \end{cases} \tag{5.10b}$$

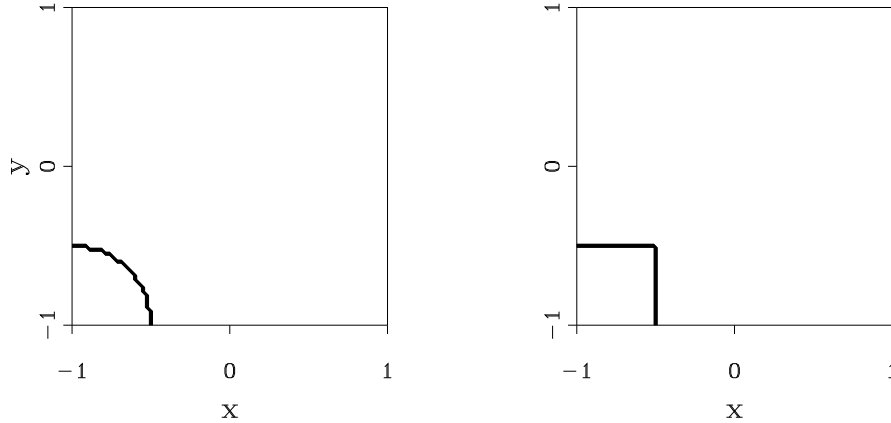For the 80×80-grid, the iso-line distributions of the initial solutions are given in Figure 16.

Figure 16: Curvilinear (left) and rectilinear (right) initial solutions (c) downstream- and upstream-facing interfaces ($h = \frac{1}{40}$).

In Figure 17, the numerical solutions at $t = 1$ are presented, as obtained with the second wrong feedback of the level-set function, without flux correction. The difference in solution quality between the downstream- and upstream-facing fronts is obvious. To show that the resolution of the downstream-facing fronts as presented in Figure 17 is really good, in Figure 18 we show the corresponding results obtained with the limited $\kappa = \frac{1}{3}$-scheme. Close observation learns that the effect of closure of cell faces in the void region does not only lead to a thinning of the interface part diffused into the void region, but also of the part diffused into the material.

To finally reduce the diffusion of upstream-facing fronts, we propose to simply apply compressive limiters. In the next section, some of these are investigated.

Compressive limiters   A well-known compressive limiter is the superbee limiter, proposed by Roe [7]:

$$\phi(r) = \begin{cases} 0, & r < 0. \\ 2r, & r < \frac{1}{2}. \\ 1, & r < 1. \\ r, & r < 2. \\ 2, & \text{else.} \end{cases} \tag{5.11}$$

By dropping the second-order accuracy property $\phi(1) = 1$, of which the usefulness is questionable for fronts, out of (5.11) we can get the simpler, even more compressive limiter

$$\phi(r) = \begin{cases} 0, & r < 0. \\ 2r, & r < 1. \\ 2, & \text{else.} \end{cases} \tag{5.12}$$
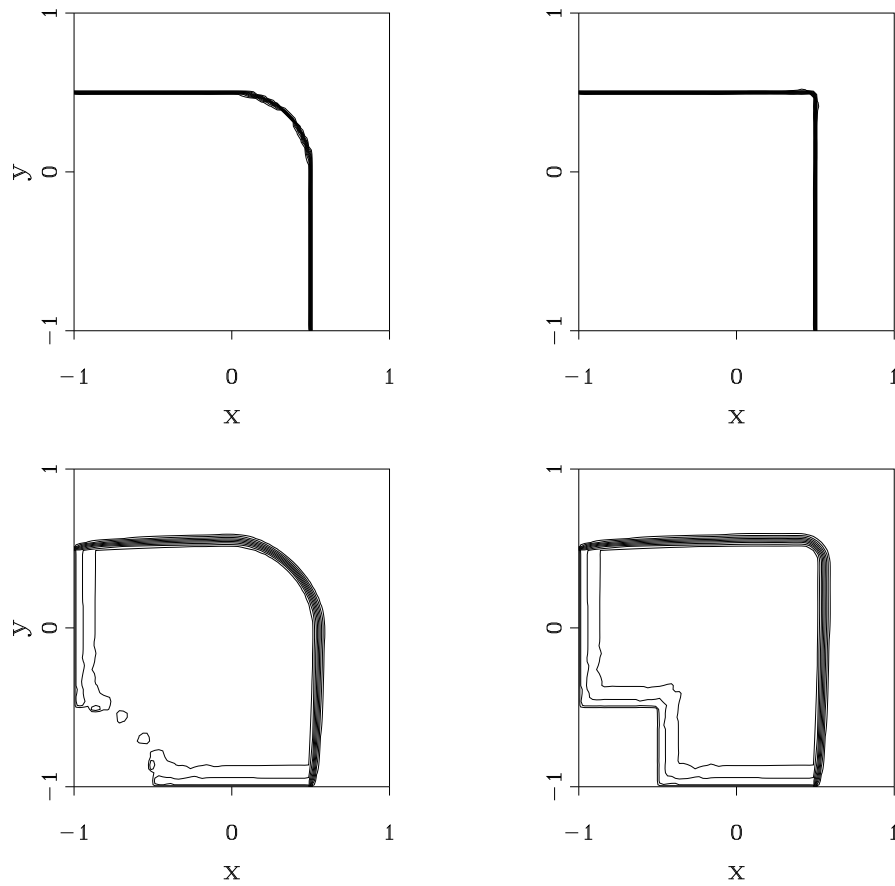
Figure 17: Curvilinear (left) and rectilinear (right) numerical solutions (c) for advection downstream-facing (up) and upstream-facing (down) interfaces with second wrong feedback of level-set function to physics (without flux correction, $h = \frac{1}{40}$).
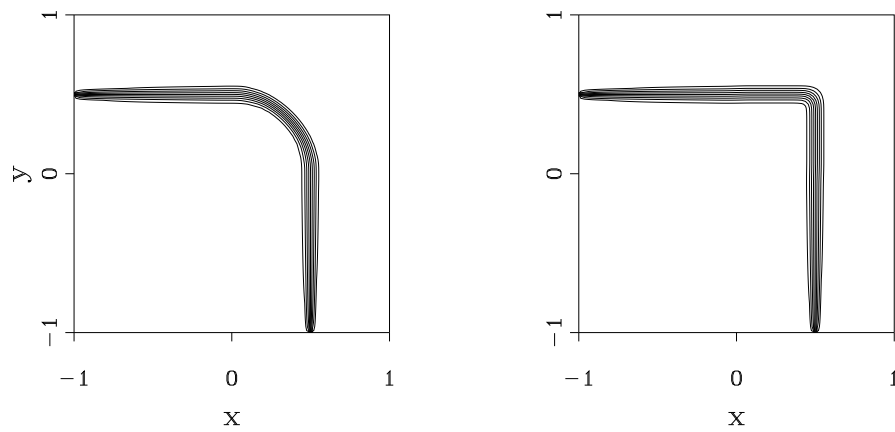

Figure 18: Curvilinear (left) and rectilinear (right) numerical solutions (c) for advection downstream-facing interfaces with limited $\kappa = \frac{1}{3}$-scheme ($h = \frac{1}{40}$).

By also dropping the (weak) monotonicity requirement $\phi(r) \leq 2$, at the risk of getting some spurious solution oscillations at the upstream-facing front, we obtain the even more compressive limiter

$$\phi(r) = \begin{cases} 0, & r < 0. \\ 2r, & \text{else.} \end{cases} \tag{5.13}$$

For the upstream-facing interfaces, numerical results for all three limiters are given in Figure 19. Comparing the results, it is clear that the superbee limiter is to be preferred. Limiters (5.12) and (5.13) are over-compressive; they falsely flatten the circular-arc front (Figure 19). Hence, the second-order accuracy condition $\phi(1) = 1$ does make sense here. Limiter (5.13) finally, also does not succeed indeed, to keep the solutions monotonous.
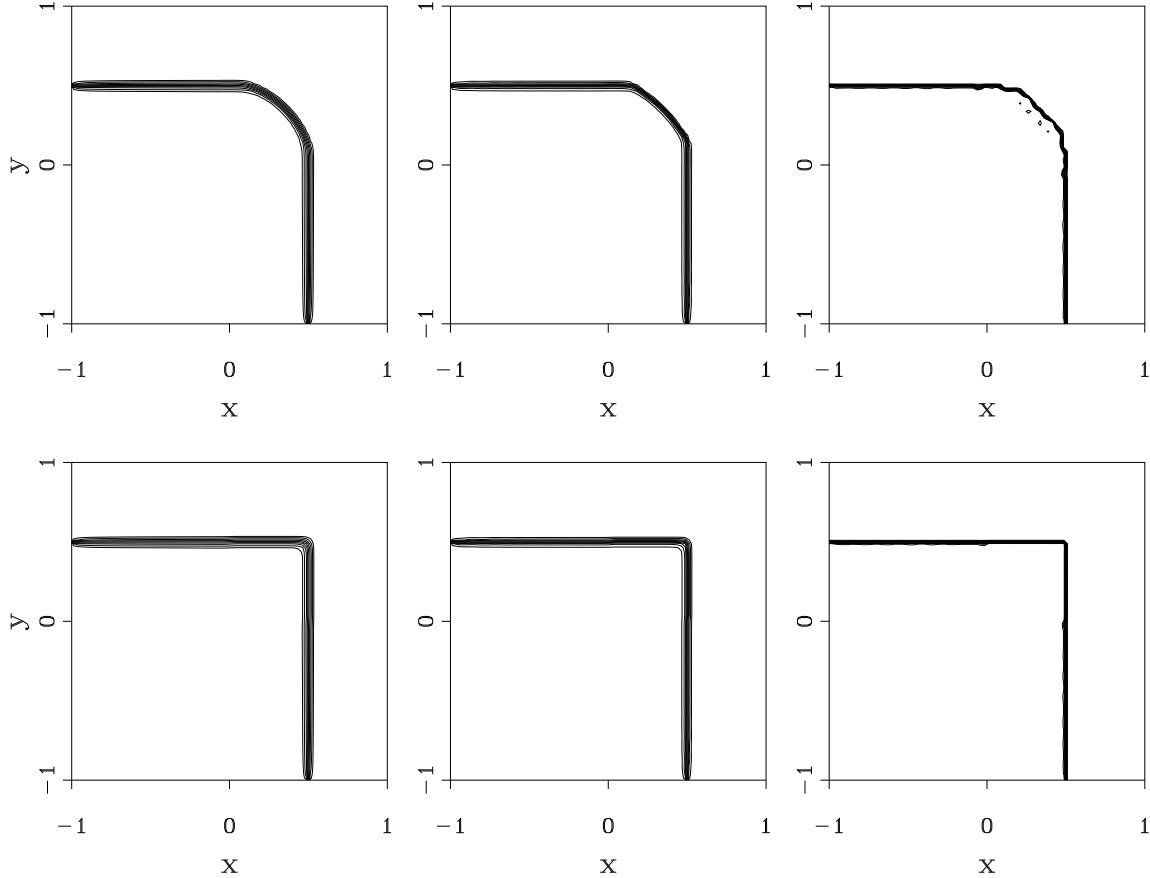

Figure 19: Numerical solutions (c) for advection upstream-facing, curvilinear (up) and upstream-facing rectilinear (down) interfaces, for $h = \frac{1}{40}$ and from left to right: superbee limiter, more compressive limiter (5.12) and most compressive limiter (5.13).

The improved coupling   Closure of cell faces will be done at the downstream sides of fronts only. Besides a front itself, its down- and upstream sides can also be accurately distinguished by means of the level-set function. In 2-D, the downstream region is there where

$$(u, v) \cdot \nabla \psi < 0. \tag{5.14}$$

The required cell-face gradient $\nabla \psi$ can be evaluated in more or less the standard second-order accurate way, as described in, for example, Section 3.7 in [6]. For the present simple test problems (with all

horizontal cell faces aligned to the x-axis and all vertical cell faces aligned to the y-axis, and with the grid equidistant and $h_x = h_y = h$), this gradient evaluation becomes, at the vertical cell faces:

$$(\nabla\psi)_{i+\frac{1}{2},j} = \left(\begin{array}{l} \left(\frac{\partial\psi}{\partial x}\right)_{i+\frac{1}{2},j} = \left\{ \begin{array}{ll} i=0: & \frac{1}{3h}(-8\psi_{\frac{1}{2},j} + 9\psi_{1,j} - \psi_{2,j}) \\ i=n: & \frac{1}{3h}(8\psi_{n+\frac{1}{2},j} - 9\psi_{n,j} + \psi_{n-1,j}) \\ \text{else}: & \frac{1}{h}(\psi_{i+1,j} - \psi_{i,j}) \end{array} \right. \\ \\ \left(\frac{\partial\psi}{\partial y}\right)_{i+\frac{1}{2},j} = \left\{ \begin{array}{ll} j=1: & \frac{1}{2h}(-5\psi_{i+\frac{1}{2},1} + 8\psi_{i+\frac{1}{2},2} - 3\psi_{i+\frac{1}{2},3}) \\ j=n: & \frac{1}{2h}(5\psi_{i+\frac{1}{2},n} - 8\psi_{i+\frac{1}{2},n-1} + 3\psi_{i+\frac{1}{2},n-2}) \\ \text{else}: & \frac{1}{2h}(\psi_{i+\frac{1}{2},j+1} - \psi_{i+\frac{1}{2},j-1}) \end{array} \right. \end{array} \right), \quad (5.15a)$$

and at the horizontal cell faces:

$$(\nabla\psi)_{i,j+\frac{1}{2}} = \left(\begin{array}{l} \left(\frac{\partial\psi}{\partial x}\right)_{i,j+\frac{1}{2}} = \left\{ \begin{array}{ll} i=1: & \frac{1}{2h}(-5\psi_{1,j+\frac{1}{2}} + 8\psi_{2,j+\frac{1}{2}} - 3\psi_{3,j+\frac{1}{2}}) \\ i=n: & \frac{1}{2h}(5\psi_{n,j+\frac{1}{2}} - 8\psi_{n-1,j+\frac{1}{2}} + 3\psi_{n-2,j+\frac{1}{2}}) \\ \text{else}: & \frac{1}{2h}(\psi_{i+1,j+\frac{1}{2}} - \psi_{i-1,j+\frac{1}{2}}) \end{array} \right. \\ \\ \left(\frac{\partial\psi}{\partial y}\right)_{i,j+\frac{1}{2}} = \left\{ \begin{array}{ll} j=0: & \frac{1}{3h}(-8\psi_{i,\frac{1}{2}} + 9\psi_{i,1} - \psi_{i,2}) \\ j=n: & \frac{1}{3h}(8\psi_{i,n+\frac{1}{2}} - 9\psi_{i,n} + \psi_{i,n-1}) \\ \text{else}: & \frac{1}{h}(\psi_{i,j+1} - \psi_{i,j}) \end{array} \right. \end{array} \right). \quad (5.15b)$$

Now we can give the final discretization. At the vertical cell faces we take:

$\psi_{i+\frac{1}{2},j}$ according to (4.1a),

$$\psi_{i+\frac{1}{2},j} < \psi_f : \left\{ \begin{array}{ll} \nabla\psi_{i+\frac{1}{2},j} \text{ according to (5.15a)}, \\ (u,v)\cdot\nabla\psi_{i+\frac{1}{2},j} < 0 : & c_{i+\frac{1}{2},j} \text{ according to (5.6a).} \\ \text{else:} & c_{i+\frac{1}{2},j} \text{ according to (2.6a) and (5.11).} \end{array} \right. \quad (5.16a)$$

else: $\qquad\qquad\qquad\qquad\qquad\qquad c_{i+\frac{1}{2},j}$ according to (2.6a) and (2.7).

And, similarly, at the horizontal cell faces we take:

$\psi_{i,j+\frac{1}{2}}$ according to (4.1b),

$$\psi_{i,j+\frac{1}{2}} < \psi_f : \left\{ \begin{array}{ll} \nabla\psi_{i,j+\frac{1}{2}} \text{ according to (5.15b)}, \\ (u,v)\cdot\nabla\psi_{i,j+\frac{1}{2}} < 0 : & c_{i,j+\frac{1}{2}} \text{ according to (5.6b).} \\ \text{else:} & c_{i,j+\frac{1}{2}} \text{ according to (2.6b) and (5.11).} \end{array} \right. \quad (5.16b)$$

else: $\qquad\qquad\qquad\qquad\qquad\qquad c_{i,j+\frac{1}{2}}$ according to (2.6b) and (2.7).

In Figure 20, numerical results are presented for this level-set approach with improved coupling. For both the advection of the circle and the square, the spray in the wake has disappeared. A flaw in the solutions obtained for the advected square is the crosswise diffusion at the diagonally opposite corner points where the discretization changes type. A fix to this will probably be to make the transition between both schemes smoother. In the Tables 3a and 3b (p. 22), we give some quantitative information about the numerical solutions. In comparison with the results given in Table 1, an improvement of $\|\Delta c\|_1$ has been obtained.
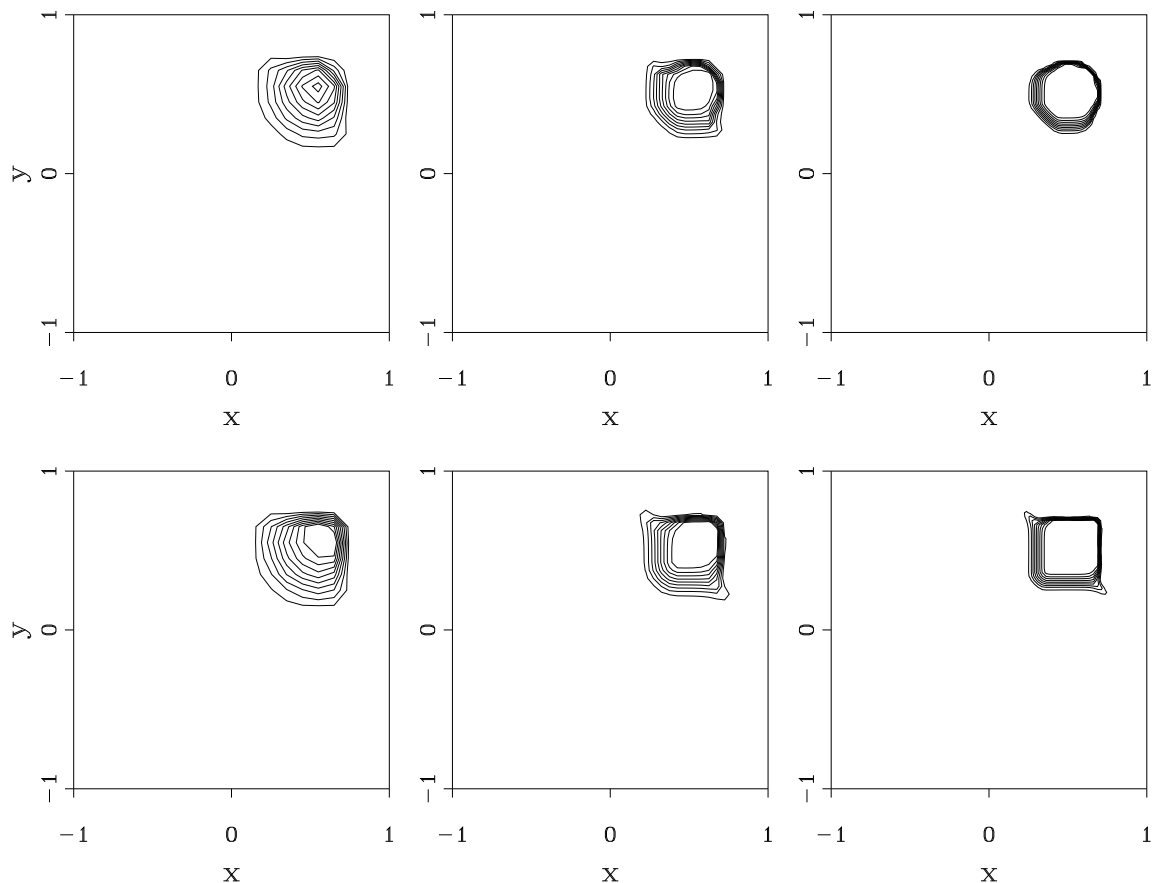
Figure 20: Numerical solutions (c) for advection circle (up) and square (down) with improved coupling scheme, for from left to right: $h = \frac{1}{10}, \frac{1}{20}, \frac{1}{40}$.

6. Conclusions

For capturing free boundaries in an Eulerian formulation, the advantages of level-set methods over most alternative Eulerian techniques are:

- Level-set methods are smooth at physical discontinuities and − hence − allow us to maintain maximum numerical accuracy there.

- Through the level-set function, the location of the discontinuity is clearly defined. As opposed to a discontinuous function, the level-set function has a single and unique value there.

- The level-set function can be simply embedded in the system of physical equations and can be discretized collectively (and thus consistently) with these.

- There is no principal difficulty in extending a level-set method from 2-D to 3-D.

- The possibility exists to advect the level-set function as an active (instead of as a passive) scalar, i.e., to directly feed it back into the discretization of the physical equations.

Based on the model studies presented in this paper, the following foreknowledge exists for the development of a level-set method for material-void interfaces. For shape-tracking purposes, already without feedback of the level-set function into the physics, the approach yields excellent results.

When feeding information about the level-set function back into the discretization of the physical equations, for downstream-facing material-void interfaces strongly improved non-geometrical results can be obtained as well (viz., by closing all cell faces in the void region downstream of the front). For upstream-facing fronts, so far, the gains obtained through feedback are modest. Here, the level-set method is still open for further research. For problems with both downstream- and upstream-facing fronts, the challenge is to properly combine three different discretizations: that in the upstream void region, that in the downstream void region and that in the material domain. Given the foregoing list of advantages, further research is worth the effort.

Circle	$h = \frac{1}{10}$	$h = \frac{1}{20}$	$h = \frac{1}{40}$
$\|\Delta c\|_1$	3.2×10^{-2}	1.7×10^{-2}	9.7×10^{-3}
$\|\Delta c\|_\infty$	5.7×10^{-1}	5.0×10^{-1}	5.1×10^{-1}
Square	$h = \frac{1}{10}$	$h = \frac{1}{20}$	$h = \frac{1}{40}$
$\|\Delta c\|_1$	3.6×10^{-2}	2.0×10^{-2}	1.2×10^{-2}
$\|\Delta c\|_\infty$	5.5×10^{-1}	6.2×10^{-1}	6.4×10^{-1}

Table 1: Numerical results for advection circle (up) and square (down) with limited $\kappa = \frac{1}{3}$-scheme.

Circular	$h = \frac{1}{10}$	$h = \frac{1}{20}$	$h = \frac{1}{40}$
$\|\Delta \psi\|_1$	9.5×10^{-3}	1.5×10^{-3}	1.9×10^{-4}
$\|\Delta \psi\|_\infty$	1.6×10^{-1}	3.4×10^{-2}	4.8×10^{-3}
Square	$h = \frac{1}{10}$	$h = \frac{1}{20}$	$h = \frac{1}{40}$
$\|\Delta \psi\|_1$	1.4×10^{-2}	4.4×10^{-3}	1.4×10^{-3}
$\|\Delta \psi\|_\infty$	1.5×10^{-1}	9.3×10^{-2}	5.0×10^{-2}

Table 2: Numerical results for advection circular (up) and square (down) level-set function with limited $\kappa = \frac{1}{3}$-scheme.

Circle	$h = \frac{1}{10}$	$h = \frac{1}{20}$	$h = \frac{1}{40}$
$\|\Delta c\|_1$	2.0×10^{-2}	1.1×10^{-2}	5.4×10^{-3}
$\|\Delta c\|_\infty$	5.4×10^{-1}	5.7×10^{-1}	5.5×10^{-1}
Square	$h = \frac{1}{10}$	$h = \frac{1}{20}$	$h = \frac{1}{40}$
$\|\Delta c\|_1$	2.0×10^{-2}	1.3×10^{-2}	7.2×10^{-3}
$\|\Delta c\|_\infty$	5.9×10^{-1}	6.0×10^{-1}	6.7×10^{-1}

Table 3: Numerical results for advection circle and square with final scheme.

References

1. C. Aalburg, Experiments in minimizing numerical diffusion across a material boundary, *MSc-thesis* (Department of Aerospace Engineering, University of Michigan, Ann Arbor, 1996). Also: http://www.engin.umich.edu/research/cfd/publications/publications.html

2. A.J. Chorin, Flame advection and propagation algorithms, *J. Comput. Phys.* **35** (1980) 1–11.

3. F.H. Harlow and J.E. Welch, Numerical calculation of time-dependent viscous incompressible flow of fluid with free surfaces, *Phys. Fluids* **8** (1965) 2182–2189.

4. C.W. Hirt and B.D. Nicholls, Volume of fluid (VOF) method for dynamics of free boundaries, *J. Comput. Phys.* **39** (1981) 201–225.

5. B. Koren, A robust upwind discretization method for advection, diffusion and source terms, in: C.B. Vreugdenhil and B. Koren, Eds., *Numerical Methods for Advection-Diffusion Problems*, *Notes on Numerical Fluid Mechanics* **45** (Vieweg, Braunschweig, 1993) 117–138.

6. R. Peyret and T.D. Taylor, *Computational Methods for Fluid Flow* (Springer, Berlin, 1983).

7. P.L. Roe, Some contributions to the modelling of discontinuous flows, in: B.E. Engquist, S. Osher, and R.C.J. Somerville, Eds., *Large-Scale Computations in Fluid Mechanics*, *Lectures in Applied Mathematics* **22, Part 2** (American Mathematical Society, Providence, Rhode Island, 1985) 163–193.

8. J.A. Sethian, *Level Set Methods: Evolving Interfaces in Geometry, Fluid Mechanics, Computer Vision, and Materials Science* (Cambridge University Press, Cambridge, 1996).

9. J.E. Welch, F.H. Harlow, J.P. Shannon and B.J. Daly, The MAC method, *Report LA-3425* (Los Alamos Scientific Laboratory, Los Alamos, New Mexico, 1966).

24

Table of Contents